International Journal of Women's Health

Dovepress
Taylor & Francis Group

Open Access Full Text Article

ORIGINAL RESEARCH

Antifungal, Antibiofilm and Anticytotoxic Properties of Biogenic CuO Nanoparticles Derived From *Moringa oleifera* Leaves Against Vaginal Candidiasis

Mohammad Zubair[1,2], Yazeed Albalawi[3], Roba Alatawy[1,2]

[1]Department of Medical Microbiology, Faculty of Medicine, University of Tabuk, Tabuk, Kingdom of Saudi Arabia; [2]Molecular Microbiology and Infectious Disease Research Unit, University of Tabuk, Tabuk, Kingdom of Saudi Arabia; [3]Department of Obstetrics and Gynecology, Faculty of Medicine, University of Tabuk, Tabuk, Kingdom of Saudi Arabia

Correspondence: Mohammad Zubair, Email zmohammad@ut.edu.sa

Objective: *Moringa oleifera* leaf extract can mediate green synthesis of metal oxide nanoparticles with potential antimicrobial properties. This study evaluated copper oxide nanoparticles (CuO NPs) synthesized using *M. oleifera* for antifungal, antibiofilm, and cytocompatibility effects in a vaginal-simulant medium.

Methods: CuO NPs were synthesized using *M. oleifera* leaf extract and characterized by FT-IR, XRD, UV–Vis, SEM, and EDX. 10 *Candida albicans* isolates and ATCC 90028 were screened for biofilm production; strong biofilm producers were selected for detailed testing. Antifungal activity (viability assays, MIC_{50}, MIC_{90}, MFC) and dose–response relationships were determined. Effects at sub-inhibitory concentrations on EPS production, cell-surface hydrophobicity, membrane permeability, ROS generation, germ tube formation, and biofilm formation/disruption were assessed. In vitro biocompatibility was evaluated by MTT assays on L929 fibroblasts, RAW 264.7 macrophages, MCF-12F epithelial cells, PBMCs, and by hemolysis assay.

Results: CuO NPs produced a concentration-dependent reduction in *Candida* viability with high dose–response correlation (R^2 = 0.967–0.9779). MIC_{50}, MIC_{90}, and MFC values ranged 44.5–103 µg/mL (ATCC 90028: MIC_{50} 44.5 µg/mL, MIC_{90} 86.5 µg/mL, MFC 91 µg/mL; *C. albicans* 6: MIC_{50} 51.5 µg/mL, MIC_{90} 79.5 µg/mL, MFC 103 µg/mL). At sub-inhibitory concentrations, CuO NPs reduced EPS production and cell-surface hydrophobicity, increased membrane permeability and ROS generation, inhibited germ tube formation, and limited biofilm formation and integrity. Biocompatibility testing showed concentration-dependent cytotoxicity in fibroblasts and macrophages at higher doses, relative tolerance of MCF-12F cells, low hemolysis, and acceptable PBMC viability at lower concentrations.

Conclusion: *M. oleifera*-mediated CuO NPs exhibit potent in vitro antifungal and antibiofilm activity against *C. albicans* and affect multiple virulence-related pathways, with a distinguishable therapeutic window based on cell-type–dependent cytotoxicity. These findings support further development and optimization of topical intravaginal formulations of green-synthesized CuO NPs for candidal biofilm-associated infections, with additional in vivo safety and efficacy studies needed.

Keywords: *Moringa oleifera*, vaginal candidiasis, CuO nanoparticles, antifungal, anti-biofilm

Introduction

Recurrent vulvovaginal candidiasis is a significant global health concern. An estimated 138 million women experience recurrent episodes each year (range 103–172 million). This corresponds to a global annual prevalence of 3871 per 100,000 women, and an estimated 372 million women suffer recurrent vulvovaginal candidiasis over their lifetime.[1] Acute infection episodes reduce the health-related quality of life and impose significant personal and societal costs. Even during acute episodes, many women reported ongoing discomfort and anxiety. Moreover, they are associated with reduced productivity and impaired daily functioning.[2] These observations demonstrate the urgent need for improved preventive and therapeutic approaches.

Received: 14 September 2025
Accepted: 21 November 2025
Published: 2 December 2025

Graphical Abstract

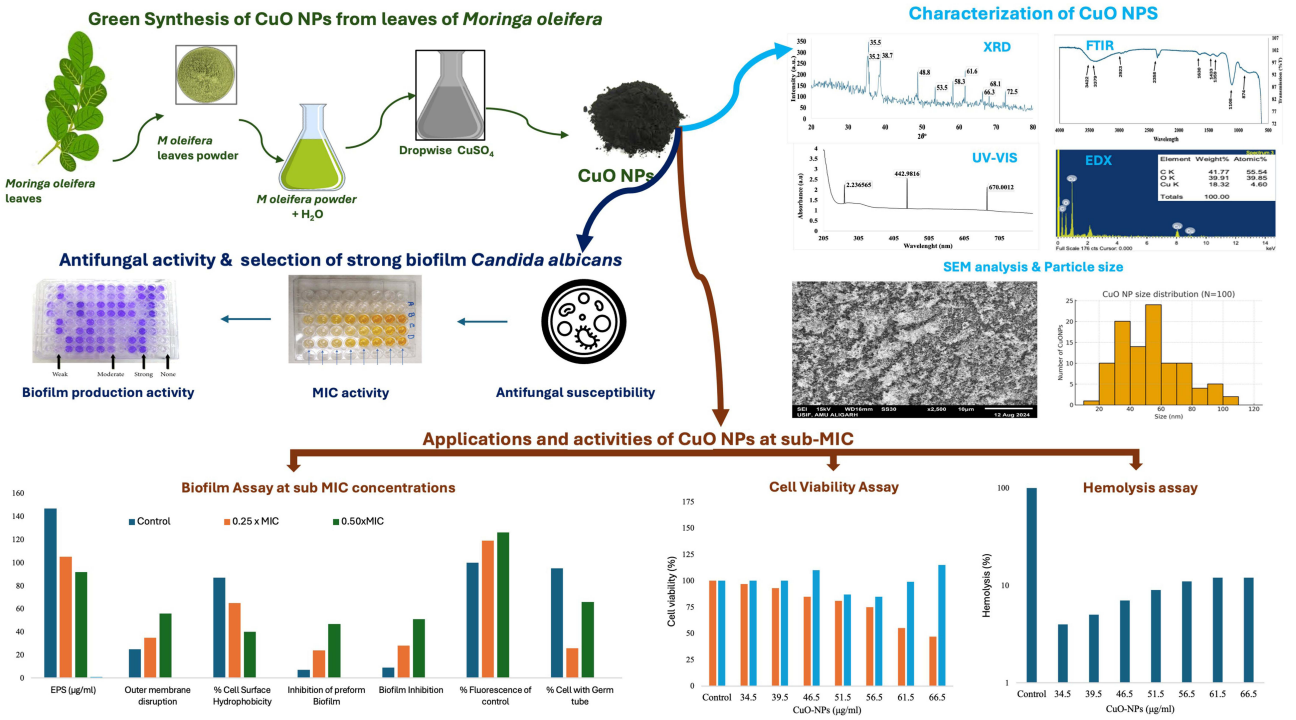

Vaginal candidiasis is most commonly caused by polymorphic opportunistic *Candida albicans*, although non-albicans *Candida* species are increasingly implicated. Clinical manifestations include vulvar and vaginal erythema, excoriation, swelling, and a thick white adherent discharge.[3] The pathogenic success of *Candida spp*. reflects multiple virulence attributes, including adhesion to epithelial surfaces, morphological switching, secretion of hydrolytic enzymes, and ability to form biofilms.[4] Biofilm formation leads to increased tolerance to conventional antifungal agents.[5]

Current therapy for vulvovaginal candidiasis relies on topical or systemic antifungal agents such as azoles, polyenes, echinocandins, acrylamides, and nucleoside analogs. Although many patients respond to these agents, the treatment of recurrent or drug-resistant infections remains problematic. For example, triazole therapy frequently requires prolonged or repeated courses that extend for months to a year to achieve sustained remission.[6] Despite extensive treatment, relapse is a common occurrence. Several factors limit the clinical efficacy of the conventional vaginal drug administration. These include poor diffusion over the vaginal mucosal surface, restricted contact with lesions located within the vaginal folds, and inadequate penetration into deeper tissue layers where hyphae may persist. The vaginal mucus can trap drug molecules and impede their distribution. This can further reduce therapeutic concentrations at the site of infection.[6] These limitations highlight the need for delivery strategies to increase local drug bioavailability and reduce systemic exposure.

Nanoparticle-based delivery systems have several attractive features for the management of vaginal infections. Nanocarriers can improve drug dispersion and mucosal absorption, provide sustained release, reduce the required dosage, and lower local and systemic toxicity.[6] These properties make nanotechnology an important platform for developing effective interventions for recurrent and refractory vaginal candidiasis.

Nanoparticle properties, such as size, shape, chemical composition, and surface chemistry, determine their biological interactions and fate. NPS have a much larger specific surface area and higher surface energy because they are orders of magnitude smaller than bulk materials. Factors such as particle size distribution, morphology (including crystal form and surface roughness), and surface charge (which can be modified by coatings or capping agents) determine the colloidal stability, dissolution rate, and how particles bind to cells and biomolecules.[7]

Smaller nanoparticles are more likely to cross biological barriers and enter cells, whereas particle morphologies, such as rods versus spheres, can lead to different cellular uptake routes and intracellular trafficking. Surface chemistry, including functional groups, coatings, and adsorbed biomolecules, affect NPs' binding affinity, stability, and biocompatibility of NPs in biological environments. The surface charge also influences the interactions between NPs and cells. Positively charged NPs show greater cellular uptake but can cause higher cytotoxicity than neutral or negatively charged particles.[8] These interconnected parameters must be carefully controlled to achieve the desired antimicrobial or drug delivery effects of nanoparticles while simultaneously limiting toxicity.[7]

Copper-based nanoparticles have attracted considerable attention as cost-effective antimicrobial agents. Copper is inexpensive and copper-containing nanomaterials have demonstrated broad antimicrobial activity in different settings. Copper-based nanoparticles have demonstrated antifungal effects against a range of organisms, including phytopathogenic fungi. This shows their potential as affordable alternatives to conventional antifungals.[9]

Most nanoscale metals are produced using chemical methods that can have unintended consequences such as high energy consumption, environmental pollution, and possible health risks. To address these problems, green synthesis has been developed. Instead of harsh industrial chemicals, plant extracts have been used to reduce metal ions. Compared to conventional chemical approaches, green synthesis is cheaper, generates less pollution, and is safer for both the environment and human health.[10] *Moringa oleifera* has emerged as a versatile biological resource for nanoparticle syntheses. Extracts from the leaves, flowers, stems, peels, and pods of *M. oleifera* are rich in flavonoids, phenolics, polysaccharides, and terpenoids, which function as reducing, stabilizing, and capping agents, respectively, during nanoparticle formation. Nanoparticles synthesized from *M. oleifera* components have displayed a range of biological activities, including antibacterial, antioxidant, and anticancer effects.[11]

Vaginal simulant medium (VSM) that mimics the physiological vaginal environment is most often used for in vitro testing. VSM reproduces physicochemical properties of the vaginal mucosa. This creates a biomimetic environment for the evaluation of the antifungal activity. Unlike standard laboratory media, VSM is more complex and includes components of vaginal fluids such as glycogen, mucin, and albumin.[12,13] Previous studies have indicated that using simulated vaginal fluid improves the clinical relevance of antifungal assays by recreating mucosal conditions.[12]

To our knowledge, no previous study has examined biogenic copper oxide (CuO) nanoparticles or vaginal *Candida* isolates from northern Tabuk. In this preliminary study, we synthesized CuO nanoparticles using *Moringa oleifera* leaf extract, characterized their physicochemical properties, evaluated their antifungal activity against clinically relevant *Candida* isolates (planktonic and biofilm forms), and assessed their cytotoxicity toward vaginal epithelial cells. These initial data will lead to larger, more definitive investigations into the potential of biogenic CuO nanoparticles as cost-effective, environment-friendly therapies for vulvovaginal candidiasis.

Materials and Methods

Ethical Consideration

The study protocol was approved by the Local Research Ethics Committee (LREC) the University of Tabuk (approval no. UT-642-419-2025) in accordance with the National Committee of Bioethics (NCBE), Kingdom of Saudi Arabia. Informed consent was obtained from all patients and controls for voluntary participation.

Clinical Samples: Inclusion Criteria, Collection and Isolate Identification

Female patients aged 18–40 years presenting to the Prince Fahad Specialist Hospital (PFSH), Tabuk, Saudi Arabia with culture-confirmed vaginal candidiasis were screened. Patients were eligible if they had not received systemic antifungal therapy within the preceding 20 days; were able to provide informed consent; and were not immunocompromised, pregnant, breastfeeding, or allergic to copper compounds. Ten *Candida albicans* isolates were recovered and confirmed by the hospital microbiology laboratory following international guidelines.

Antifungal Susceptibility Testing (Disk Diffusion)

Antifungal susceptibility was assessed by disk diffusion according to CLSI.[14] The following agents (HiMedia, India) were tested: amphotericin B (50 µg), itraconazole (30 µg), fluconazole (25 µg), ketoconazole (10 µg), voriconazole (10 µg) and nystatin (100 U). Zones of inhibition were measured in millimeters and interpreted as susceptible or resistant. *C. albicans* ATCC 90028 served as a quality control strain.

Biofilm Screening and Selection of Isolates

Biofilm formation was quantified in 96-well flat-bottom microplates as described by Zubair et al.[15] Assays were carried out in triplicate, and mean absorbance at 590 nm (OD_{590}) was recorded. The isolates were classified as weak (0.100-–0.400), moderate (0.401–0.800) or strong (> 0.800) biofilm producers.

Preparation of Biological Reducing Agent and CuO Nanoparticles

Fungal-Derived Reducing Agent (Culture Supernatant)

To prepare a fungal derived reducing agent, several *Candida spp*. strains were cultured in potato dextrose broth (PDB) (Ingredients Gms / Litre Potatoes, infusion from 200.000 Dextrose 20.000 Final pH (at 25°C) 5.1±0.2. Briefly, 25 µL of cell suspension (1×10^6 cells/mL) was inoculated into 250 mL PDB and incubated at 30 °C, 120 rpm for 72 h. biomass was harvested by filtration, washed three times with deionized water, and incubated in 250 mL deionized water under the same conditions for an additional 72 h. The culture supernatant was collected by filtration through a 0.22 µm nitro-cellulose membrane, stored at 4 °C, or used immediately.

CuO Nanoparticles Synthesis

The collection of fresh *Moringa oleifera* leaves was meticulously executed to guarantee the high-quality representative samples for the study was identified by Prof Nasir M Khan of Faculty of Applied, University of Tabuk, and subsequently preserved at the ultra-low temperature storage facility of the Department of Medical Microbiology. Leaves were washed with deionized (DI) water to remove dust, surface contaminants, and other impurities. The cleaned leaves were oven-dried at 60 °C for 6 h to remove residual moisture without altering phytochemical constituents. The dried material was finely ground using a laboratory-grade grinder to obtain a homogeneous powder.[16]

For extract preparation, 10 g of powdered leaves was boiled in 100 mL of DI water for 15 min at 80 °C and filtered through Whatman No. 1 filter paper to obtain a clear aqueous extract. A 10 mL aliquot of this extract was immediately mixed with 100 mL of 10 mM $CuSO_4 \cdot 5H_2O$ solution (Sigma-Aldrich, USA) under continuous magnetic stirring at 700 rpm for 24 h at room temperature. The reaction mixture was monitored for the color transformation from light blue to dark brown. This color change indicates the formation of CuO NP.[17]

The resulting colloidal suspension was centrifuged at 10,000 rpm for 10 min to collect NPs. The pellet was washed three times with DI water to remove unreacted copper ions and residual phytochemicals. After Subsequently, it was oven-dried overnight at 60 °C overnight. The dried CuO NPs were carefully scraped, stored in airtight glass vials, and preserved for further characterization and experimental use.

Characterization of CuO NPs

The synthesized CuO nanoparticles were characterized using complementary physicochemical and spectroscopic techniques to confirm their successful synthesis, surface functionality, crystallinity, morphology, and elemental composition:[18,19]

- UV–Visible spectroscopy (UV-Vis): The optical properties and surface plasmon resonance (SPR) band of the nanoparticles were examined using a UV-3600 Plus double-beam spectrophotometer (Shimadzu, Kyoto, Japan) in the wavelength range 200–800 nm. The characteristic absorption peak of the CuO NPs was monitored to confirm nanoparticle formation.
- Fourier Transform Infrared Spectroscopy (FTIR): Functional groups responsible for the reduction, stabilization, and surface capping of CuO NPs were analyzed using an ALPHA-E FTIR spectrometer (Bruker, Billerica, MA, USA). Spectra were recorded in the range of 4000–400 cm^{-1} to identify the phytochemical signatures bound to the nanoparticle surface.

- X-ray Diffraction (XRD) The crystalline nature and average crystallite size of the CuO NPs were determined using an XRD-6000 diffractometer (Shimadzu, Japan) operated with Cu Kα radiation (λ = 1.5406 Å) at 40 kV and 30 mA. Data were recorded over the 2θ range of 10°–80°, and the diffraction peaks were compared with standard JCPDS files to confirm the monoclinic phase of CuO.
- Field-Emission Scanning Electron Microscopy (FESEM) with Energy-Dispersive X-ray Spectroscopy (EDX) and the morphological features and particle size distribution were visualized using a Nova Nano FEG-SEM 45 (FEI, USA). Elemental analysis was performed using an attached EDX detector, confirming the presence of copper and oxygen signals and excluding major impurities.

Preparation of CuO NP Suspension for Biological Assays

Vaginal simulant medium (VSM; Sigma-Aldrich, India) was used to model the vaginal environment in vitro. A 10 mg/mL stock suspension of CuO NPs was prepared by adding 100 mg of nanoparticles to 10 mL of VSM. This was followed by gentle shaking and sonication (100 W, 40 kHz) for 30 min with 30-s pulses every 2 min.

In Vitro Antifungal Assays in Vaginal Simulant Medium (VSM)

Broth Microdilution (MIC and MFC)

The minimum inhibitory concentration (MIC) and minimum fungicidal concentration (MFC) were determined in VSM by broth microdilution following the CLSI M27-A2 guidelines, with minor modifications.[20] In each well of a 96-well plate, 50 µL of *C. albicans* inoculum (1.5×10^5 CFU/mL) was combined with 50 µL of serially diluted CuO NPs (0–128 µg/mL). Concentrations tested to refine the MIC ranged from 0 to 103 µg/mL in 6.5 µg/mL increments. The final volume was adjusted to 100 µL using a cell-free VSM. Controls contained inocula without nanoparticles and sterility controls contained only VSM. Plates were incubated at 37 °C and read at 24 and 48 h. MIC was defined as the lowest concentration preventing visible growth, with absorbance measured at 550 nm. For MFC, 10 µL from each well at 48 h was plated onto Sabouraud dextrose agar. The MFC had the lowest concentration, yielding ≥ 99.9% reduction in colony-forming units compared to the initial inoculum, whereas reductions < 99.9% were identified as fungistatic. *C. albicans* ATCC 90028 was used as a reference.

Antimicrobial Dose-Response and Selection For Sub-MIC Experiments

Dose-response curves were generated for the clinical biofilm isolates (identified as strong producers) and ATCC 90028. Nonlinear curve fitting (quadratic or other appropriate models) was used to determine the relationship between CuO NPs concentration and cell viability. The coefficients of determination (R^2) were used to assess reproducibility. The clinical isolate that showed the most reproducible response was selected for subsequent sub-MIC antibiofilm assays.

Sub-MIC Functional Assays

All sub-MIC functional assays in this study were performed in vaginal simulant medium (VSM) to mimic the physiological environment of *Candida albicans* and ensure the biological relevance of the observed nanoparticle effects.

Biofilm Inhibition

Microtiter plate wells were inoculated with *Candida albicans* in VSM and treated with CuO NPs at 0.75× MIC, 0.50× MIC, and 0.25× MIC concentrations. Plates were incubated at 37 °C for 48 h. Untreated wells served as controls.[15] After incubation, wells were washed with phosphate-buffered saline (PBS pH = 7.4) and stained with 100 µL of 0.1% crystal violet (Sigma-Aldrich, St. Louis, MO) for 30 min at room temperature. Excess stain was removed by rinsing, and the bound dye was solubilized to obtain the biofilm biomass in 95% ethanol. To quantify biofilm biomass, we measured the optical density of the ethanol supernatant at 590 nm.

Exopolysaccharide Production

Cell-free supernatants were collected from *Candida* cultures grown in VSM containing CuO NPs at sub-MIC levels (1:1 volume ratio) and from untreated controls. Exopolysaccharides (EPS) were precipitated by adding chilled ethanol to each supernatant in a 3:1 ethanol: supernatant ratio and incubating at 4°C for 16–18 hours. The precipitated EPS were

quantified using the Dubois colorimetric assay with a glucose standard curve for calibration.[21] Untreated cultures served as controls. All assays were performed in triplicate. The mean weight of the EPS precipitate was recorded and the percentage reduction relative to that of the untreated control was calculated.

Cell Surface Hydrophobicity

Cell surface hydrophobicity was determined using the microbial adhesion to hydrocarbon (MATH) assay. Overnight VSM cultures (1 mL) were mixed with 100 µL of xylene and the indicated sub-MIC concentrations of CuO NPs. Untreated cultures served as controls. The samples were vortexed vigorously for 2 min, allowed to separate at room temperature for 10 min, and the absorbance of the aqueous phase was measured at 530 nm wavelength. The hydrophobicity was calculated as follows:

$$\%\ \text{Hydrophobicity}\ (1 - \text{OD after vortexing}/\text{OD before vortexing}) \times 100$$

Outer Membrane Permeability

The N-Phenyl-1-naphthylamine (NPN) uptake assay was performed to assess CuO NP-induced outer membrane disruption, as described by Shiraz et al.[22] Biofilm-facilitating *C. albicans* cells were treated with sub-MIC concentrations of CuO NPs in VSM (1 mL total) and incubated at 37°C for 60 minutes. Thereafter, cells were washed and resuspended in 1 mL of 0.5% NaCl. A 200 µL aliquot was mixed with NPN (final concentration 0.75 mM made from 100 mM ethanol stock), and fluorescence was measured (excitation 350 nm, emission 420 nm) at room temperature. Untreated cultures were used as controls. The percentage uptake was determined as follows:

$$\%\ \text{NPN uptake} = (\text{Fobs} - \text{F0})/(\text{F100} - \text{F0}) \times 100$$

where F_obs is the observed fluorescence, F0 is the baseline fluorescence without treatment, and F100 corresponds to the fluorescence in the presence of Triton X-100.

Disruption of Preformed Biofilm

Biofilms were cultivated in 96-well plates by incubating *C. albicans* in VSM for 24 h at 37 °C. After washing wells in PBS twice, we added fresh VSM with 0.5 × MIC CuO NPs or no nanoparticles and subsequently incubated the cells for another 24 h at 37 °C. After the second wash, adherent biomass was stained with 0.1% crystal violet. Biofilm disruption was quantified by measuring the absorbance at 585 nm according to Schlichter Kadosh et al.[23]

Germ Tube Formation

Germ tube inhibition was assessed using a modified Mackenzie method.[15,24] Candida suspensions (10 mL) were incubated with 2 mL of sterile pooled sheep serum spiked with sub-MIC concentrations of CuO NPs for 3 h. The control group consisted of serum only, with no nanoparticles. Smears were prepared and 50 cells per sample were viewed under a microscope. Cells that showed germ tubes at least twice the length of the yeast cells were counted as positive.

Reactive Oxygen Species Generation

ROS production was assessed using the DCFH-DA assay according to a previously described protocol.[15] Reactive oxygen species (ROS) production was measured in *C. albicans* inoculated at 1.5×10^5 cells per well in a 96-well plate with sub-MIC CuO NPs in VSM and incubated at 37°C for 24 h. Untreated cells served as controls. After centrifugation (1500 rpm, 10 min), the cells were washed thrice with PBS. After Next, 200 µL of PBS containing 45 µM DCFDA was added to each well and incubated at 37°C for 60 minutes. Fluorescence was recorded at the excitation and emission wavelengths of 485 and 530 nm, respectively.

Biocompatibility Studies

Cell Viability Assay

The biocompatibility of the synthesized CuO NPs was evaluated using an MTT assay on four cell types: murine fibroblasts (L929), murine macrophages (RAW 264.7), human breast epithelial cells (MCF-12F), and peripheral blood mononuclear cells (PBMCs) isolated from healthy volunteer donors using Ficoll gradient centrifugation. The L929, RAW

264.7, and MCF-12F cell lines were obtained from Sigma-Aldrich (India). Cells were cultured in RPMI-1640 medium (Gibco) supplemented with 10% fetal bovine serum (Gibco) and 100 IU/mL penicillin-streptomycin (Sigma-Aldrich) at 37°C in a humidified atmosphere containing 5% CO2. Cells cultured without nanoparticles were used as controls. MTT (3-(4,5-dimethylthiazol-2-yl)-2,5-diphenyltetrazolium bromide) powder (Merck, India) was dissolved in PBS and added (20 µL) to wells seeded at 1×104 cells per well in 96-well plates, 3 h before each endpoint. CuO NPs concentrations were selected around the MIC for Candida inhibition (51.5 µg/mL ±5 µg/mL) and tested at 24, 48, and 72 h. After MTT incubation, the supernatants were removed and the formazan crystals were dissolved in 100 µL of acidic isopropanol. Absorbance at 540 nm was measured, and cell viability was expressed as a percentage of the control (set to 100%). All assays were performed in triplicate. A decrease in cell proliferation was observed at concentrations of 34.5, 39.5, and 46.5 µg/mL. The reducing agent alone exhibits no cytotoxicity.[25]

Haemolysis Assay

Haemocompatibility was assessed following ISO 10993-4[26] guidelines using the protocol devised by Garcia-Marin et al.[17] Fresh human erythrocytes (270 µL) were incubated in 96-well plates with CuO NPs at 51.5 ±5 µg/mL (three concentrations) in DMEM (final volume 300 µL). Wells without nanoparticles were used as controls. After incubation for 1 h at 37°C and 5% CO_2, plates were centrifuged at 3000 rpm for 5 min. The supernatants were transferred to new 96-well plates, and the absorbance at 541 nm was measured using a UV-visible spectrophotometer (Thermo Scientific Multiskan GO, Vantaa, Finland).

Statistical Analysis

The experiments were conducted in triplicate unless otherwise indicated. The means+ standard deviation of all the obtained values are presented using SigmaPlot16. A comparison of the means of various sets of data was carried out through a *t*-test. *Significantly different ($p \leq 0.05$) from untreated control; **significantly different ($p \leq 0.005$) from untreated control.

Results

Characterisation of CuO NPs

The FT-IR spectrum of the green-synthesized CuO nanoparticles featured a pair of broad overlapping bands at 3422 and 3379 cm < ps > ^{1}, which were attributable to -OH stretching from surface-adsorbed water or hydroxyl groups. The weaker band at 2923 cm^{-1} reflects aliphatic C-H stretching of trace organic residues from the plant extract, whereas the sharp feature at 2358 cm^{-1} arises from physisorbed CO_2. The H-O-H bending vibration of coordinated water appears at 1630 cm^{-1}, and the medium-intensity bands at 1433 and 1359 cm^{-1} can be assigned to the C-H or C-O bending modes of residual biomolecules. The peak at 1108 cm^{-1} corresponds to C-O (or C-N) stretching, also from phytochemical capping agents. Finally, the distinct band at 874 cm < > B-^{1} lies in the metal-oxygen region and is characteristic of Cu-O lattice vibrations, thereby confirming the successful formation of CuO NPs (Figure 1a).

The XRD pattern displays distinct diffraction peaks at 2θ = 35.2, 35.5, 38.7, 48.8, 53.5, 58.3, 61.6, 66.3, 68.1 and 72.5°, which are characteristic of monoclinic CuO (tenorite). The absence of extra reflections attributable to metallic Cu or Cu_2O indicated that the product was phase-pure CuO. The observed peak broadening relative to the bulk references is consistent with nanocrystalline domains (typically a few tens of nanometers) and/or lattice microstrain. The closely spaced features at 35.2–35.5° likely arise from overlapping reflections or the slight lattice distortions/strain common in nanoparticles. Overall, XRD analysis confirmed the formation of crystalline, largely monophasic CuO NPs with nanoscale crystallite sizes (Figure 1b).

The UV-Vis spectrum of CuO NPs shows a very strong UV absorption at the short-wavelength end (below 300 nm) and two distinct features in the visible: sharp peaks at 442.98 nm and 670.00 nm (with a modest, nearly constant baseline through the rest of the visible). The intense UV band is typical of strong electronic (charge-transfer) absorption from the oxygen 2p → copper 3d states, while the feature near 443 nm is most consistent with the interband/charge-transfer transitions in nanoscale CuO. The weaker band at 670 nm likely arises from the localized d-d transitions of Cu^{2}+ or from surface/defect states introduced by the nanoparticle surface. The overall broad visible absorption and the presence of these discrete bands are consistent with nanoscale defect-rich CuO, which can absorb UV-visible wavelengths (Figure 1c).

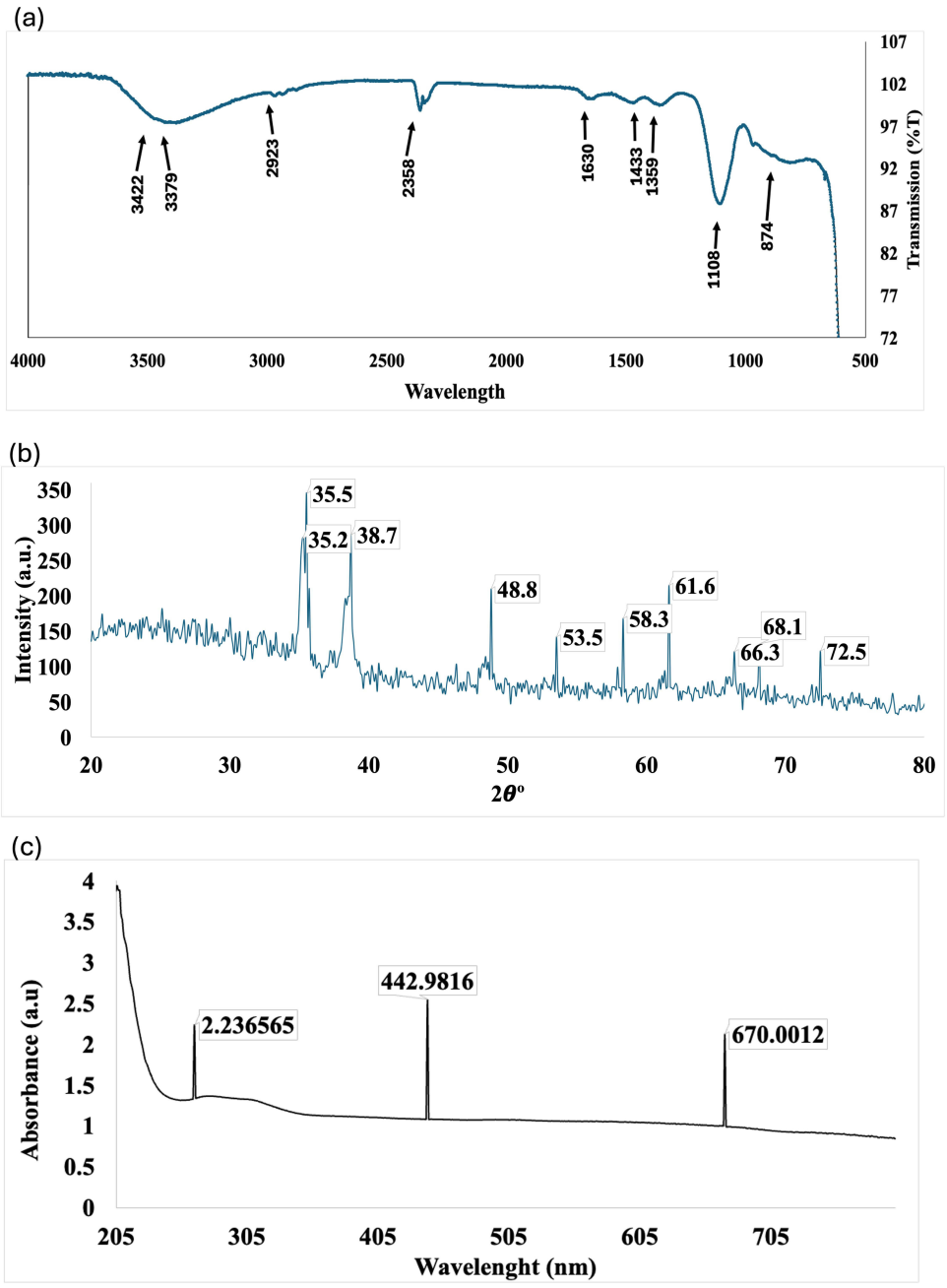

Figure 1 (**a**) FTIR, (**b**) XRD, and (**c**) UV-Vis spectra of CuO nanoparticles.

The SEM series showed that the product was composed of densely packed irregular nanoscale crystallites that formed larger cauliflower-like agglomerates. At low magnification (Figure 2A and B), the film appeared continuous and highly textured and composed of many fused clusters. At intermediate magnifications (Figure 2C and D), these clusters were resolved into plate/flake-like or petal-like subunits with clear interparticle voids and a rough surface topology. At the highest magnification (Figure 2E), individual nanoscale sheets/grains and sharp edges were visible, confirming a polycrystalline, anisotropic morphology.

The histogram of CuO NPs lengths, calculated from 100 individual measurements using the ImageJ software, showed a size distribution ranging from 15 to 104 nm (Figure 2F). The majority of the particles were clustered in the 40–60 nm range. The overall mean particle size based on individual measurements was approximately 51.7 ± 21.0 nm. This broad distribution suggests that the nanoparticles are polydisperse. Both smaller (<30 nm) and larger (>90 nm) particles were present in smaller proportions.

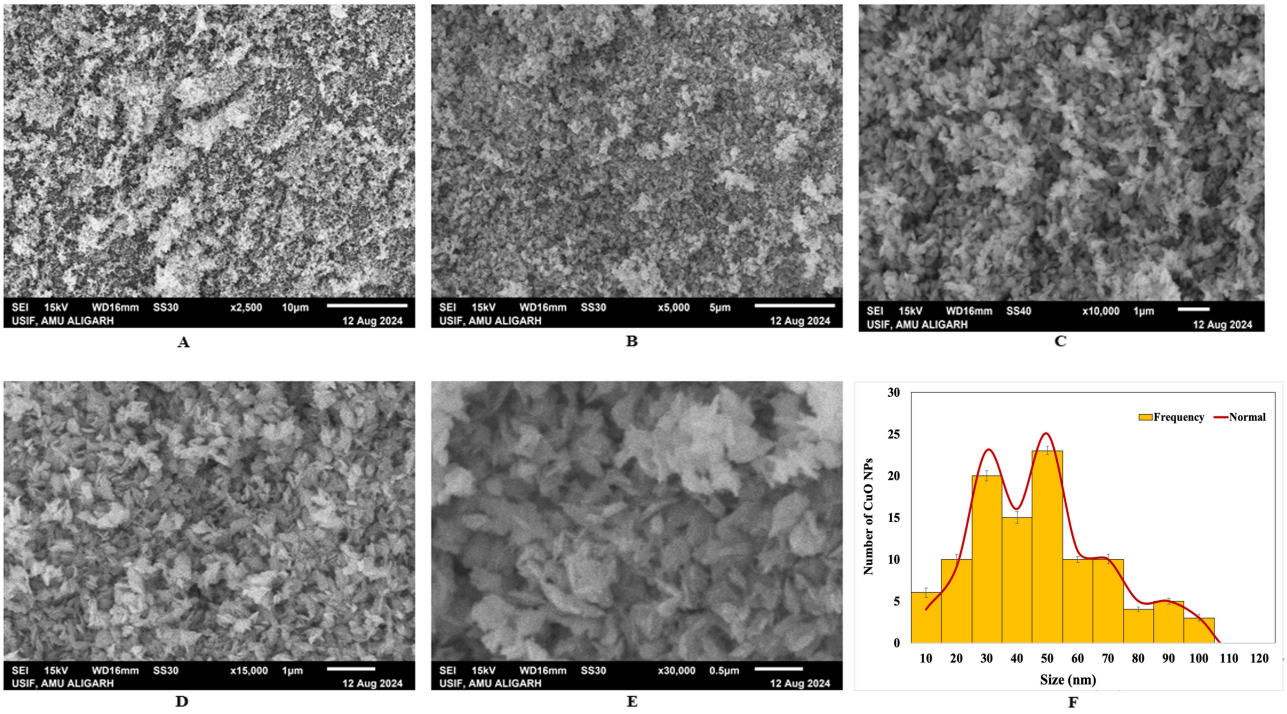

Figure 2 SEM analysis of CuO nanoparticles at: (**A**) ×2500, (**B**) ×5000, (**C**) ×10000, (**D**) ×15000, (**E**) ×30000, and (**F**) Histogram of nanoparticles.

Figure 3 shows the EDAX spectrum, with clear signals for carbon, oxygen, and copper. The inset table shows the weight percentages of C 41.77, O 39.91, and Cu 18.32, and the atomic percentages of C 55.54, O 39.85, and Cu 4.60, for a total of 100. The simultaneous presence of copper and oxygen peaks confirms the formation of a copper oxide phase.

Antifungal Susceptibility

The antibiogram of 10 *Candida albicans* isolates showed that most strains remained susceptible to the tested azoles (itraconazole, ketoconazole, and voriconazole) and polyenes (nystatin and amphotericin B), but resistance was observed in a subset of isolates (Table 1). Three isolates (1, 2, and 6) were resistant to fluconazole with high MICs/MFCs (MIC = 64 μg/mL, MFC = 80 μg/mL), whereas single isolates were resistant to ketoconazole (isolate 4; MIC 16 μg/mL, MFC 24 μg/mL), voriconazole (isolate 5; MIC 4 μg/mL, MFC 5 μg/mL), and amphotericin B (isolate 7; MIC 2 μg/mL, MFC 3.3 μg/mL). Four isolates (3, 8, 9, and 10) were susceptible to all tested agents and had no MIC/MFC determined (ND).

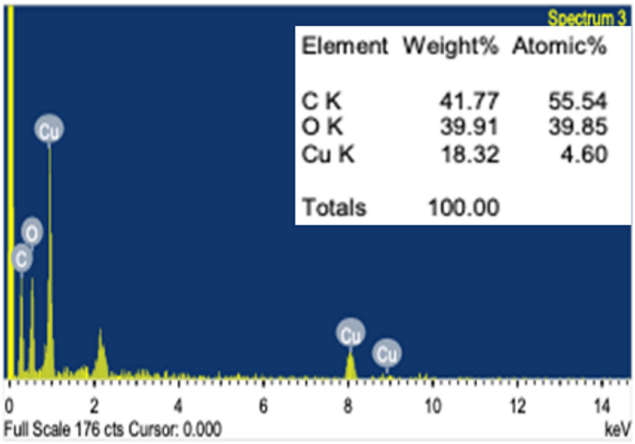

Figure 3 EDAX analysis of CuO nanoparticles.

https://doi.org/10.2147/IJWH.S567527

Table 1 Antibiogram of *Candida Albicans*

Candida albicans	Sensitive	Resistant	MIC	MFC
Isolate 1	Itr, Ket, Vor, Nys, AmpB	Flu	64 µg/mL	80 µg/mL
Isolate 2	Itr, Ket, Vor, Nys, AmpB	Flu	64 µg/mL	80 µg/mL
Isolate 3	Flu, Itr, Ket, Vor, Nys, AmpB	ND	ND	ND
Isolate 4	Flu, Itr, Vor, Nys, AmpB	Ket	16 µg/mL	24 µg/mL
Isolate 5	Flu, Itr, Ket, Nys, AmpB	Vor	4 µg/mL	5 µg/mL
Isolate 6	Itr, Ket, Vor, Nys, AmpB	Flu	64 µg/mL	80 µg/mL
Isolate 7	Flu, Itr, Ket, Vor, Nys	AmpB	2 µg/mL	3.3 µg/mL
Isolate 8	Flu, Itr, Ket, Vor, Nys, AmpB	ND	ND	ND
Isolate 9	Flu, Itr, Ket, Vor, Nys, AmpB	ND	ND	ND
Isolate 10	Flu, Itr, Ket, Vor, Nys, AmpB	ND	ND	ND

Notes: Tested concentration ranges: Flu 0.125–64 µg/mL; Nys 0.06–32 µg/mL; Itr, Ket, Vor and AmpB 0.016–16 µg/mL.
Abbreviations: MIC, minimum inhibitory concentration; MFC, minimum fungicidal concentration; ND, not determined; Flu, fluconazole; Itr, itraconazole; Ket, ketoconazole; Vor, voriconazole; Nys, nystatin; AmpB, amphotericin B.

Selection of Biofilm-Producing Isolates

The Biofilm screening of 10 *Candida albicans* isolates showed that 2 isolates (20%) were strong biofilm producers, 4 (40%) were intermediate, 1 (10%) was weak, and 3 (30%) produced no biofilm (Table 2). Strong biofilm producers (*C. albicans* 1 and 6) were selected for the antibiofilm activity of CuO NPs, along with the reference strain *C. albicans* ATCC 90028.

Antimicrobial Activity of CuO NPs

Figure 4 shows the concentration-dependent loss of *C. albicans* viability in response to CuO nanoparticles for all three strains. Viability remained unchanged at the lowest dose (≤12 µg/mL) and then began to decline at 26–38 µg/mL. At 52 µg/mL, the cultures showed a substantial reduction and further increased to 64–78 µg/mL lead viability in the 10–40% range, with almost complete loss at ≥91–103 µg/mL. The fitted dose–response curves were highly consistent (R^2 = 0.967–0.978). This indicates low scatter and good reproducibility. The three curves overlap, which implies comparable susceptibility between the clinical isolates and the reference strain. At intermediate concentrations (38–64 µg/mL), *C. albicans* 1 tended to retain slightly higher viability, whereas ATCC 90028 tended to show lower viability. However, these differences were small relative to the overall pattern. *C. albicans* 6 provided the tightest fit (R^2 = 0.9779) with a smooth, monotonic decline and was selected for subsequent sub-MIC antibiofilm assays.

MIC and MFC Determination

Table 3 shows that CuO NPs have antifungal activity against both the reference strain (*C. albicans* ATCC 90028) and biofilm-positive clinical isolate (*C. albicans* 6). The ATCC strain had a lower MIC_{50} (44.5 µg/mL) than that of the clinical isolate (51.5 µg/mL). This indicates that it was slightly more susceptible to the 50% inhibition level. However, the clinical isolate reached MIC_{90} at a lower concentration (79.5 vs 86.5 µg/mL). The MFC was higher for biofilm-positive isolates (103 vs 91 µg/mL). This suggests that, although most of the clinical population is inhibited at comparable doses, a higher

Table 2 *C. Albicans* Categorized as Strong, Intermediate, Weak or Non-Biofilm Producers

	Strong n (%)	Intermediate n (%)	Weak n (%)	Non-Biofilm Producers n (%)
C. albicans N=*10*	2 (20)	4 (40)	1 (10)	3 (30)

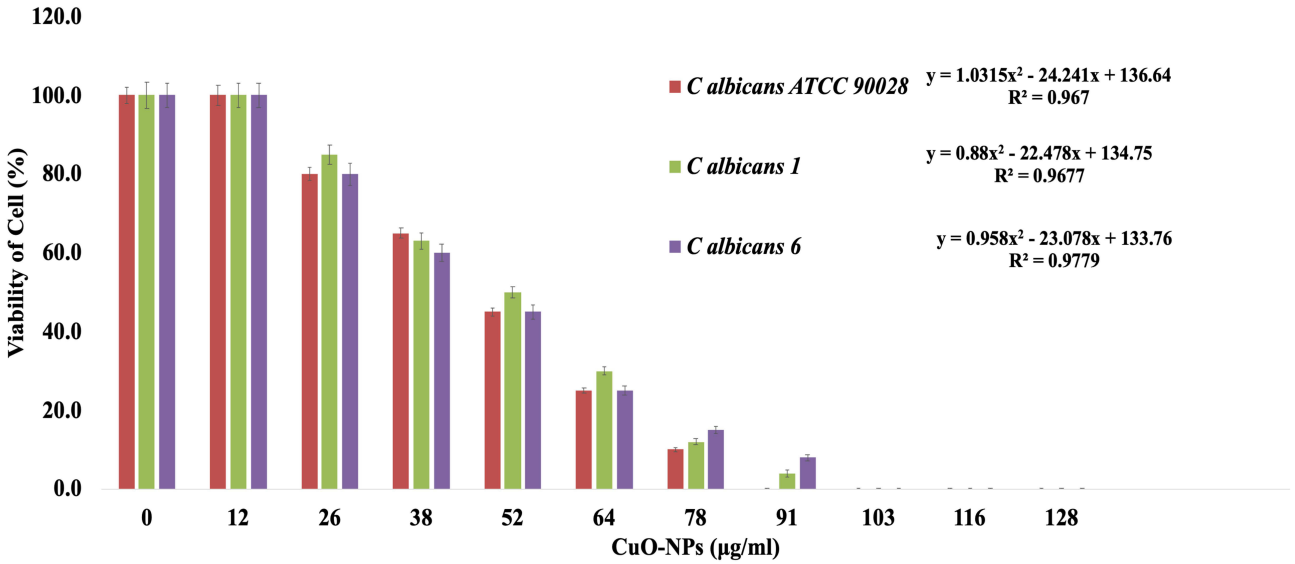

Figure 4 Antimicrobial activity of CuO against *C. albicans* (ATCC 90028), *C. albicans* 1 and *C. albicans* 6, with varying minimum inhibitory concentrations (MIC) in VSM.

concentration is required to achieve complete killing. Overall, CuO NPs were active against both strains, but the biofilm-positive isolate showed greater tolerance to fungicidal concentrations.

Antimicrobial Effects of MIC and Sub-MIC Levels of CuO NPs

Figure 5 shows that sub-inhibitory concentrations of CuO NPs produced changes in *C. albicans* physiology and biofilm behavior compared to untreated controls. Extracellular polymeric substance (EPS) production decreased in the presence of CuO (blue control, highest; red, 0.25×MIC; green, 0.5×MIC, progressively lower). This shows that, even below the MIC, the particles reduce the matrix material available for the biofilm structure.

The membrane integrity and surface properties were measured in opposite directions. Outer membrane disruption increased with CuO (lowest in control, higher at 0.25×MIC, and highest at 0.5×MIC), and % cell-surface hydrophobicity reduced substantially with treatment. These changes were consistent with the nanoparticle-induced membrane perturbation and reduced adhesive potential. Both the prevention (inhibition of biofilm formation) and reduction of established biofilms (inhibition of preformed biofilms) were enhanced by CuO in a concentration-dependent manner. This again supports the anti-biofilm effect observed at the sub-MIC levels.

Reactive oxygen species generation increased with nanoparticle exposure, with fluorescence values increasing from the control baseline (100) to 115 at 0.25×MIC and 125 at 0.5×MIC. Germ tube formation was suppressed at 0.25×MIC and remained lower than that of the control at 0.5×MIC. This indicates a non-linear or assay-dependent response to the morphological transition.

Error bars show reproducibility and asterisks indicate statistically significant differences from the control (single and double asterisks denote higher levels of significance); therefore, the majority of these changes are unlikely to reflect

Table 3 MIC50, MIC90, and MFC Values for CuO NPs Against Biofilm-Positive *C. Albicans* 6 and Standard *C. Albicans* (ATCC 90028) in VSM

	MIC 50 µg/mL	MIC 90 µg/mL	MFC µg/mL
C. albicans ATCC 90028	44.5	86.5	91
C. albicans 6	51.5	79.5	103

Abbreviations: MIC50, minimum inhibitory concentration that inhibits 50% of growth, expressed in µg/mL; MIC90, minimum inhibitory concentration that inhibits 90% of growth, expressed in µg/mL; MFC, minimum fungicidal concentration that results in 100% killing, expressed in µg/mL.

https://doi.org/10.2147/IJWH.S567527

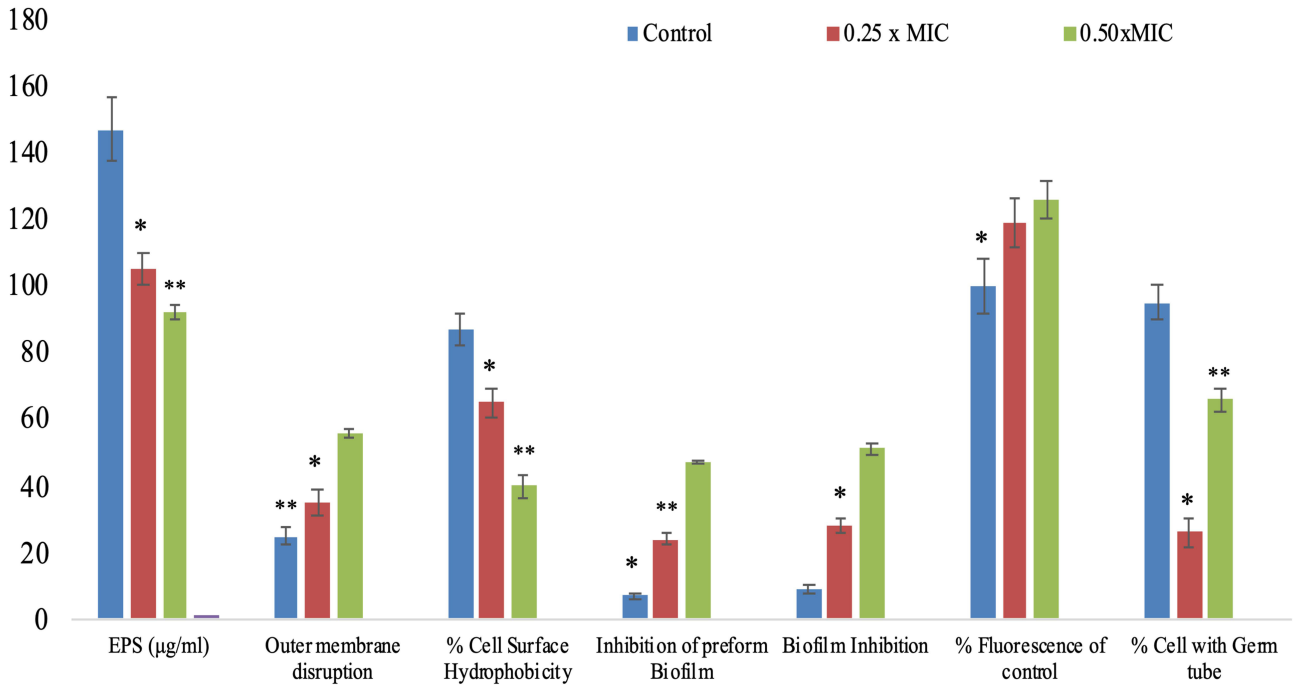

Figure 5 Effect of CuO NPs Sub-MIC on *C. albicans* physiology and biofilm behaviour. The axis for EPS demonstrates EPS production, outer membrane disruption in % disruption, % cell surface hydrophobicity in percent decrease in hydrophobicity, inhibition of pre-form biofilm in % inhibition, biofilm inhibition in % inhibition, % fluorescence, and % cell with germ tube in % reduction in germ tube formation. *Significantly different ($p \leq 0.05$) from untreated control; **significantly different ($p \leq 0.005$) from untreated control.

random variation. Overall, the figure demonstrates that CuO nanoparticles at sub-MIC concentrations impaired important virulence-related traits of *C. Albicans* such as EPS production, surface hydrophobicity, and filamentation, while increasing membrane disruption and biofilm susceptibility.

Biocompatibility Studies

Cell Viability Assay

The viability data in Figure 6 show clear concentration- and cell-type–dependent cytotoxicity of the biosynthesized CuO nanoparticles in all four cell models. Fibroblasts (panel A), macrophages (panel B) and PBMCs (panel D) show a progressive, dose-dependent loss of viability as CuO NP concentration increases from 34.5 to 66.5 µg/mL. The largest decrease was observed at the highest dose, and several reductions reached statistical significance. This pattern was more pronounced in the macrophages and fibroblasts.

In contrast, the breast epithelial cell line (panel C) did not exhibit the same pattern of decline. Instead, it showed an increase in the viability readout at low to mid CuO NP concentrations (a hormetic-like response), with only a small decrease at the highest concentrations. Some increases were statistically significant, indicating that these epithelial cells may transiently upregulate metabolic activity or proliferative signalling in response to sub-toxic nanoparticle exposure before toxicity manifests itself.

Together, these results indicated that the biosynthesized CuO NPs were cytotoxic in a concentration- and cell-specific manner, with immune cells and fibroblasts being more vulnerable at higher concentrations, whereas MCF-12F epithelial cells showed transient stimulation at lower doses.

Haemolysis Assay

Figure 7 shows the effect of CuO NPs on red blood cell (RBC) hemolysis. Control reaches 100% hemolysis. This indicated complete RBC lysis and served as the assay reference. All CuO NP treatments produced far lower hemolysis than the positive control and showed a clear concentration-dependent increase. At the lowest tested concentration (34.5 µg/mL) hemolysis is minimal, then rises progressively through the mid concentrations (39.5–51.5 µg/mL) to

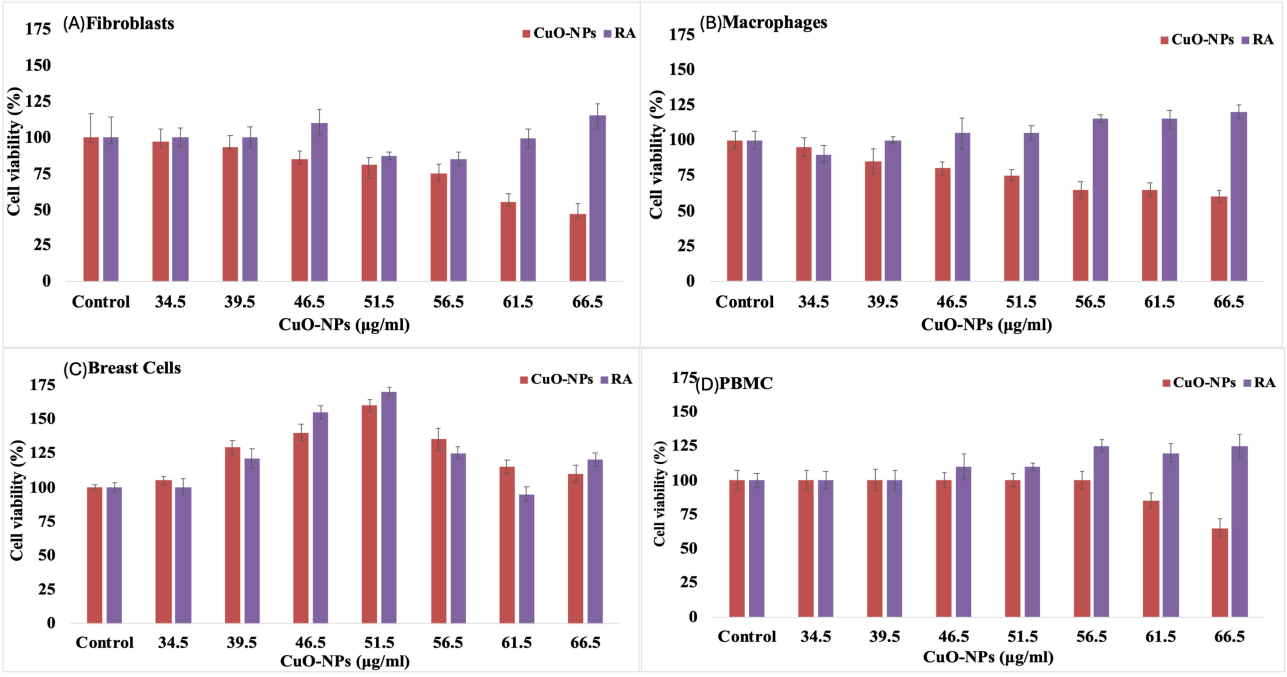

Figure 6 Cell viability assay in: (**A**) fibroblasts (L929), (**B**) macrophages (RAW 264.7), (**C**) breast cells (MCF-12F) and (**D**) Peripheral blood mononuclear cells (PBMC) exposed to biosynthesized CuO NPs.

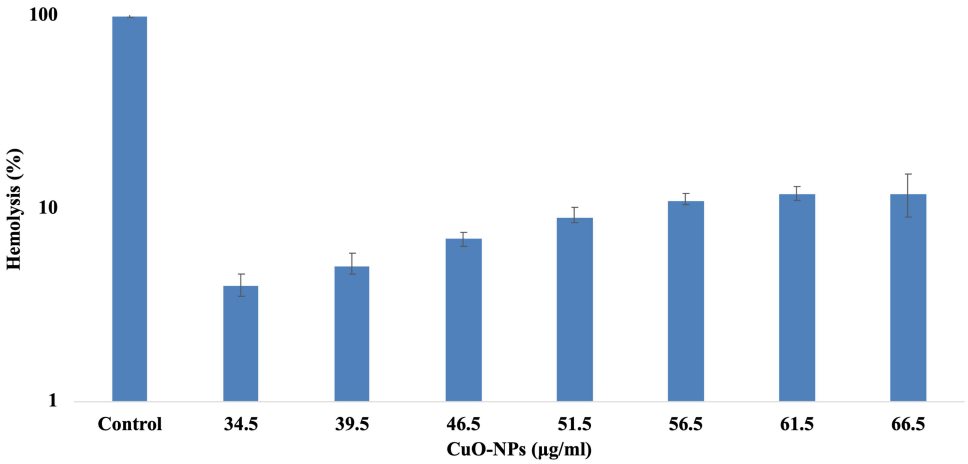

Figure 7 Effect of CuO NPs on hemolysis of red blood cells (RBC).

reach the highest values at 56.5–66.5 µg/mL. Error bars are small across replicates. This indicated consistent and reproducible measurements. Overall, within the concentration range tested, CuO NPs caused only mild dose-dependent hemolysis rather than extensive RBC destruction.

Discussion

This study employed a green synthetic approach using *Moringa oleifera* leaf extract to produce CuO nanoparticles (CuO NPs) and assessed their potential as antifungal, antibiofilm, and cytocompatible treatments for vaginal candidiasis. Physicochemical analyses confirmed that the biosynthesized CuO NPs were crystalline and were coated with phytochemicals. In the FT-IR spectrum, the broad O-H bands (3420 and 3379 cm^{-1}) and C-H/C-O bands (2923, 2358, 1630, 1433, 1359, 1108 cm^{-1}) are indicative of residual biomolecules on the nanoparticle surface. This is consistent with

https://doi.org/10.2147/IJWH.S567527

previous reports showing that plant-mediated CuO NPs display organic functional group peaks from the capping agents.[26,27] The distinct Cu-O lattice vibration at 874 cm^{-1} further confirms the formation of CuO.

XRD patterns showed only tenorite CuO reflections, with peak broadening indicative of nanoscale crystallites, mirroring other green synthesis studies reporting monophasic CuO NPs.[28] The UV-Vis spectrum showed a strong UV absorbance and distinct visible bands at 442.98 nm and 670 nm, matching the charge-transfer and defect-state transitions expected for nanocrystalline CuO. Bai et al[27] also observed a CuO NP absorbance peak near 430 nm when using *M. oleifera* extract, which is in agreement with our 442.98 nm feature. The SEM images revealed that the NPs formed textured cauliflower-like aggregates of fused nanoflakes. EDAX confirmed the presence of carbon, oxygen, and copper with a high carbon content and organic capping. Overall, these characterization data demonstrated the successful synthesis of phytochemically capped CuO NPs.

Antifungal assays showed that these CuO NPs had strong dose-dependent activity against *Candida albicans*. Moreover, many of our clinical vaginal isolates were resistant to the standard azole antifungals. This reflects the growing clinical problem of fluconazole resistance in *C. albicans*, which is historically rare, affecting fewer than 5% of isolates from RVVC cases. However, its prevalence has increased in the recent years.[29] In our study, three of the 10 isolates were fluconazole-resistant, demonstrating the need for alternative therapies.

The CuO NPs significantly reduced *Candida* viability, with MIC_{50} values around 45–52 µg/mL and MIC_{90} around 80–90 µg/mL. These potencies are comparable to or better than those reported for CuO NPs. For instance, Garcia-Marin et al[17] found complete inhibition of *C. albicans* at 39.9 µg/mL, whereas Padmavathi et al[28] reported a 100% inhibition at 150 µg/mL. Thus, our CuO NPs were at least as effective, likely exhibiting differences in particle size or surface chemistry. Moreover, the CuO NPs killed both the reference and fluconazole-resistant strains, suggesting that they act via mechanisms that bypass conventional resistance. Metal nanoparticles are known to attack fungi through multiple mechanisms (ion release, oxidative stress, membrane disruption, etc).[30] We observed dose-dependent increases in ROS levels and membrane permeabilization in *C. albicans*, consistent with this multi-target action. Padmavathi et al[28] showed that the sub-MIC of CuO NPs (50 µg/mL) prevented *C. albicans* from switching to hyphae by eliciting strong ROS production. Similarly, Garcia-Marin et al[17] observed an approximately two-fold increase in ROS levels with 33 µg/mL CuO NPs. These results confirm that oxidative damage is an important antifungal mechanism of CuO NPs.

CuO NPs also exhibit antibiofilm and antivirulence effects at sub-MIC doses. In the treated cultures, EPS (extracellular polymeric substance) production and cell surface hydrophobicity were greatly reduced, and germ tube formation was inhibited. These changes translate into significant inhibition of biofilm formation and removal of established biofilms. Such antivirulence is crucial, as *C. albicans* biofilms are a major factor in recurrent candidiasis and drug resistance.[31] Our findings are supported by previous studies on metal nanoparticles. Jalal et al[32] found that biosynthesized silver NPs nearly abolished *C. albicans* germ tube formation (97% reduction at 250 µg/mL) and almost completely prevented biofilm formation. In our study, germ tube incidence dropped from 95% in controls to 25–65% at 0.25–0.5×MIC, a strong suppression, even at sublethal doses. This aligns with reports that CuO NPs can completely block hyphal development at higher concentrations.[33]

NPs' significant impairment of EPS production and adhesion by CuO NPs is consistent with observations from other metal NPs studies, which showed that AgNPs curb biofilm matrix synthesis.[32] In our study, EPS quantity fell 40–55% at 0.25–0.5×MIC, and the percentage of membrane-disrupted cells rose in parallel, indicating destabilization of fungal cell envelopes. Collectively, these results indicated that CuO NPs target biofilm-related phenotypes by disrupting cell adhesion, matrix formation, and morphological switching. Similar antibiofilm efficacies have been reported previously. Khalaf et al[34] reported that 100 µg/mL of CuO NPs eradicated 47–66% of preformed *Candida* biofilms, whereas we saw roughly 25–50% inhibition at 0.25–0.5×MIC. Thus, our data confirmed that *M. oleifera* CuO NPs can significantly inhibit *Candida* biofilms and virulence at doses well below the fungicidal levels.

Biocompatibility tests showed that CuO NPs were reasonably safe for mammalian cells at antifungal doses. In fibroblasts and macrophages, the viability declined at higher nanoparticle concentrations. In contrast, the breast cell line (MCF-12F) remained unaffected or slightly stimulated, suggesting selective tolerance of host-like cells. These trends mirror those reported by other researchers on green CuO NPs. Garcia-Marin et al[17] observed fibroblast and macrophage viability >75% up to 35 µg/mL CuO NPs, with significant toxicity only above 37 µg/mL. Our findings also indicated that

cytotoxicity occurred at concentrations above the MIC range. The red blood cell assay showed only mild hemolysis (<15% at the highest dose), which was far below the 100% control lysis. Garcia-Marin et al[17] found <5% hemolysis up to 40 μg/mL, so our somewhat higher hemolytic effect may reflect a larger NP dose or different assay conditions. Nonetheless, hemolysis was modest, even at high doses, suggesting reasonable hemocompatibility. Overall, CuO NPs displayed a therapeutic window; fungicidal doses caused limited damage to host cells, consistent with the notion that fungi are more susceptible to ROS and membrane disruption than mammalian cells.

CuO NPs exhibited antifungal and antibiofilm effects against *C. albicans* (including drug-resistant strains) while maintaining acceptable safety in human cells. These attributes, along with the eco-friendly synthesis, demonstrate the value of biogenic CuO nanoparticles as cost-effective agents for treating recurrent vaginal candidiasis.

The CuO activity must be viewed alongside that of other metal NPs. In a comparative study of MgO, ZnO, SiO_2, and CuO NPs, the lowest MIC and MFC values were observed for ZnO NPs. This indicates that ZnO may have stronger fungicidal activity.[35] Likewise, silver nanoparticles (AgNPs) are highly antifungal. Monteiro et al[36] reported an MIC of approximately 60 μg/mL for AgNPs against *C. albicans*. Clinically, a vaginal spray containing AgNPs (15 ppm) achieved 98% cure for Candida vaginitis in patients, outperforming standard clotrimazole cream.[37] Our CuO NPs (MIC > 80–90 μg/mL) showed comparable potency.

Moreover, ZnO NPs can affect *C. albicans* even at very low doses. Hosseini et al[38] reported that sub-MIC ZnO (0.02–12 μg/mL) suppressed virulence gene expression (SAP1–3) in fluconazole-resistant vaginal *C. albicans* isolates. Thus, while ZnO and Ag were potent, CuO NPs achieved similar antifungal and antivirulence effects within the same order of magnitude. In practical terms, all of these metal NPs (CuO, ZnO, and Ag) demonstrate multi-mechanistic killing (ROS generation and membrane disruption) that can overcome conventional resistance.[39,40]

Furthermore, the advantages of CuO are clear considering its safety and application. Biogenic CuO NPs have been shown to be biocompatible at effective doses. Garcia-Marín et al[26] found mammalian fibroblasts and macrophages remained 75% viable at the MIC (35 μg/mL) and hemolysis was below 5%, even at higher doses. In our experiments, cell viability decreased markedly at CuO concentrations above the fungicidal range, whereas epithelial cells (MCF-12F) showed a hormetic response.

CuO NPs offer several practical advantages in antifungal applications. They are substantially cheaper and more abundant than noble metals such as silver, making CuO NPs more economically scalable.[41] Moreover, they exert multi-targeted antifungal effects, such as the generation of reactive oxygen species, release of Cu^2+ ions, and damage to microbial membranes, which reduce the likelihood of resistance development.[28,39] Biosynthesized CuO NPs showed minimal toxicity in mammalian host cells at antimicrobial doses.[17] Similar to Ag or ZnO, CuO NPs inhibit Candida biofilm formation and virulence traits, even at sublethal concentrations, while offering these benefits with lower host risk.[28,38]

Although these results are encouraging, several limitations prevent direct translational inferences. All experiments were conducted in vitro in a vaginal simulant medium and a limited convenience group of 10 clinical *C. albicans* isolates (only two strong biofilm producers were investigated at any length). Therefore, species diversity (non-albicans *Candida* spp)., increased strain heterogeneity, and population-level susceptibility have not yet been addressed. Second, mechanistic information is limited to phenotypic tests (ROS production, membrane permeability, EPS, hydrophobicity, and germ-tube tests) without quantitative measurement of copper ion release/dissolution kinetics, intracellular copper deposition, or molecular endpoints to identify the existing antifungal pathways. Third, nanoparticle behavior characterization was performed using bulk physicochemical properties (XRD, FT-IR, UV–Vis, SEM/EDX), but did not provide higher-resolution imaging of direct NP–cell interactions, such as TEM of fungal cells and confocal localization, and failed to measure colloidal stability, aggregation state, or surface charge in VSM over time. These factors significantly affect the biological activity and safety. Fourth, biocompatibility testing utilized a restricted set of cell types and limited exposure time frames, and thus failed to represent mucosal-specific reactions, chronic or repeated exposure toxicity, reproductive or developmental toxicity, interaction with resident vaginal microbiota, or immunomodulatory activity within tissues. Fifth, the formulation, dose delivery, mucoadhesion, and release kinetics were not addressed. As a result, the therapeutic index of intravaginal products is unknown. Sixth, green synthesis methods can introduce batch-to-batch variations owing to plant extract composition differences that were not systematically quantified or standardized in this study. Lastly, the environmental fate, possible off-target toxicity, and regulatory

aspects of copper nanoparticle application were not explored here. Together, these limitations indicate that even though the work provides a good proof of principle, it is preliminary and insufficient to justify its clinical application in the absence of follow-up experiments.

Future research should concentrate on a few important priorities in order to translate this proof-of-concept. First, we will continue antimicrobial testing and progress to biologically relevant models by testing a broader, more diverse panel of *Candida* (non-albicans species), mixed-species biofilms, and ex vivo/animal models of vaginal candidiasis to determine in vivo efficacy and local tolerance. Second, we elucidated the nanoparticle behavior and mechanism through the measurement of copper ion release and colloidal stability under physiological/mucosal conditions and correlated these measurements with molecular and imaging investigations to establish how CuO NPs interact with fungal cells and induce antifungal pathways. Third, we created and evaluated mucoadhesive intravaginal formulations) with controlled release and retention and reduced epithelial exposure. Moreover, this formulation showed complete safety evaluation, such as prolonged cytotoxicity, impact on vaginal lactobacilli, repeated dose toxicity, and immunotoxicity, to establish a therapeutic window. Fourth, maximize and qualify nanoparticle synthesis to broaden the therapeutic index and provide reproducible scale-up. Lastly, we explored combination approaches with current antifungals and conducted resistance surveillance tests while starting regulatory and environmental-fate studies early to harmonize preclinical tests with safety and quality standards.

Conclusion

Copper oxide nanoparticles produced via green synthesis from *Moringa oleifera* leaf extract demonstrated reproducible antifungal and antibiofilm action against *Candida albicans*, including fluconazole-resistant clinical isolates, with a tolerable short-term safety profile in a range of mammalian cell models. CuO NPs caused a strong, concentration-dependent loss of *C. albicans* viability, with MIC_{50} 44.5 μg/mL, MIC_{90} 79.5 μg/mL and MFCs up to 103 μg/mL. In sub-inhibitory concentrations, the particles inhibited crucial virulence characteristics such as extracellular polymeric substance production, cell-surface hydrophobicity and germ-tube formation, and enhanced membrane permeability and ROS production, and both inhibited biofilm establishment and dismounted formed biofilms. Physicochemical characterization (FT-IR, XRD, UV–Vis, and SEM/EDX) showed crystalline, phytochemical-capped CuO nanoparticles with textured, anisotropic morphology, consistent with effective antifungal activity. Additionally, short-term biocompatibility testing revealed that epithelial cells (MCF-12F) withstood low to mid doses (even exerting a transient hormetic effect), whereas fibroblasts, macrophages, and PBMCs exerted concentration-dependent cytotoxicity at higher concentrations, and hemolysis was modest within the range tested. This finding implies that there is an available therapeutic window for topical use. These findings demonstrate that biogenic CuO NPs function through several complementary modes (membrane disruption, oxidative stress, and virulence inhibition), which account for their potency against drug-resistant bacteria and minimize the potential for quick resistance emergence. Clinically and on a practical basis, the low cost and environmentally friendly synthesis of CuO make them good candidates for development of topical intravaginal preparations for the treatment of recurrent or drug-refractory vulvovaginal candidiasis, after being subject to further safety, formulation and in-vivo efficacy work.

Data Sharing Statement

The data will be available to review from the corresponding author on reasonable request.

Ethics Statement

This study was approved by the Local Research Ethics Committee (LREC) of the University of Tabuk (approval no. UT-642-419-2025) in accordance with the norms of the National Committee of Bioethics (NCBE), Kingdom of Saudi Arabia. Informed consent was obtained from all patients and controls prior to participation. The study was conducted in accordance with the ethical principles of the Declaration of Helsinki.

Acknowledgments

This scientific paper is derived from a research grant funded by the Research, Development, and Innovation Authority (RDIA) – Kingdom of Saudi Arabia – with grant number 13263-Tabuk-2023-UT-R-3-1-hw. A special thanks to Prof Nasir M Khan, of Faculty of Applied college at the University of Tabuk for the identification of plant. The X-ray

diffraction (XRD) and Fourier-transform infrared spectroscopy (FTIR) analyses were performed at the Organic & Medicinal Chemistry Research Laboratory, Faculty of Science, University of Tabuk. We would like to express our deepest gratitude to the University Sophisticated Instruments Facility (USIF) of Aligarh Muslim University in Aligarh, India for granting us access to their scanning electron microscopy (SEM) equipment. These facilities allowed us to obtain the high-resolution images necessary for our study.

Author Contributions

All authors made significant contributions to the work reported, whether that is in conception, study design, execution, acquisition of data, analysis and interpretation, or in writing the manuscript and revising the manuscript; gave final approval of the version to be published; have agreed on the journal policy; and agree to be accountable for all aspects of the work.

Funding

This scientific paper is derived from a research grant funded by the Research, Development, and Innovation Authority (RDIA) – Kingdom of Saudi Arabia – with grant number 13263-Tabuk-2023-UT-R-3-1-hw.

Disclosure

The authors report no conflicts of interest in this work.

References

1. Denning DW, Kneale M, Sobel JD, Rautemaa-Richardson R. Global burden of recurrent vulvovaginal candidiasis: a systematic review. *Lancet Infect Dis*. 2018;18(11):e339–e347. doi:10.1016/S1473-3099(18)30103-8
2. Aballea S, Guelfucci F, Wagner J, et al. Subjective health status and health-related quality of life among women with recurrent vulvovaginal candidosis (RVVC) in Europe and the USA. *Health Qual Life Outcomes*. 2013;11(1):169. doi:10.1186/1477-7525-11-169
3. Jeanmonod R, Chippa V, Jeanmonod D. Vaginal candidiasis. In: *StatPearls*. StatPearls Publishing; 2024.
4. Macias-Paz IU, Perez-Hernández S, Tavera-Tapia A, Luna-Arias JP, Guerra-Cardenas JE, Reyna-Beltrán E. Candida albicans the main opportunistic pathogenic fungus in humans. *Rev Argent Microbiol*. 2023;55(2):189–198. doi:10.1016/j.ram.2022.08.003
5. Alikhani T, Ghazvini RD, Mirzaii M, et al. Drug resistance and biofilm formation in Candida species of vaginal origin. *Iran J Public Health*. 2022;51(4):913. doi:10.18502/ijph.v51i4.9253
6. Yang M, Cao Y, Zhang Z, et al. Low intensity ultrasound-mediated drug-loaded nanoparticles intravaginal drug delivery: an effective synergistic therapy scheme for treatment of vulvovaginal candidiasis. *J Nanobiotechnol*. 2023;21(1):53. doi:10.1186/s12951-023-01800-x
7. Abbasi R, Shineh G, Mobaraki M, Doughty S, Tayebi L. Structural parameters of nanoparticles affecting their toxicity for biomedical applications: a review. *J Nanopart Res*. 2023;25(3):43. doi:10.1007/s11051-023-05690-w
8. Vignesh A, Menaka C, Amal TC, Selvakumar S, Vasanth K. Exploring the dual impact of nanoparticles on human well-being: a comprehensive review of risks and benefits. *Next Nanotechnol*. 2025;8(100223):100223. doi:10.1016/j.nxnano.2025.100223
9. Ibarra-Laclette E, Blaz J, Perez-Torres CA, et al. Antifungal effect of copper nanoparticles against Fusarium kuroshium, an obligate symbiont of Euwallacea kuroshio ambrosia beetle. *J Fungi*. 2022;8(4):347. doi:10.3390/jof8040347
10. Ying S, Guan Z, Ofoegbu PC, et al. Green synthesis of nanoparticles: current developments and limitations. *Environ Technol Innov*. 2022;26:102336. doi:10.1016/j.eti.2022.102336
11. Perumalsamy H, Balusamy SR, Sukweenadhi J, et al. A comprehensive review on Moringa oleifera nanoparticles: importance of polyphenols in nanoparticle synthesis, nanoparticle efficacy and their applications. *J Nanobiotechnol*. 2024;22(1):71. doi:10.1186/s12951-024-02332-8
12. Bostanaru-Iliescu AC, Enache AC, Lungu II, et al. Chitosan-based hydrogels containing nystatin and propolis as a novel tool for Candida auris skin decolonization. *Gels*. 2025;11(7):498. doi:10.3390/gels11070498
13. Navarro S, Abla H, Colmer-Hamood JA, Ventolini G, Hamood AN. Under conditions closely mimicking vaginal fluid, Lactobacillus jensenii strain 62B produces a bacteriocin-like inhibitory substance that targets and eliminates Gardnerella species. *Microbiology*. 2023;169(11):001409. doi:10.1099/mic.0.001409
14. Clinical and Laboratory Standards Institute. *Performance Standards for Antimicrobial Susceptibility Testing. 30th Ed. CLSI Supplement M100*. Wayne (PA): Clinical and Laboratory Standards Institute; 2020.
15. Zubair M, Husain FM, Al-Amri M, et al. In vitro inhibition of biofilm and virulence factor production in azole-resistant strains of Candida albicans isolated from diabetic foot by Artemisia vulgaris stabilized tin (IV) oxide nanoparticles. *Front Cell Infect Microbiol*. 2024;13:1322778. doi:10.3389/fcimb.2023.1322778
16. El-Tanbouly R, Gaber MA, Omran S, et al. Moringa (Moringa oleifera) green-synthesized copper oxide nanoparticles for the drought tolerance of tomato (Solanum lycopersicum). *BMC Plant Biol*. 2025;25(1):685. doi:10.1186/s12870-025-06708-2
17. Garcia-Marin LE, Juarez-Moreno K, Vilchis-Nestor AR, Castro-Longoria E. Highly antifungal activity of biosynthesized copper oxide nanoparticles against Candida albicans. *Nanomaterials*. 2022;12(21):3856. doi:10.3390/nano12213856
18. Parekh ZR, Chaki SH, Hirpara AB, et al. CuO nanoparticles—synthesis by wet precipitation technique and its characterization. *Phys B*. 2021;610:412950. doi:10.1016/j.physb.2021.412950

19. Das PE, Abu-Yousef IA, Majdalawieh AF, Narasimhan S, Poltronieri P. Green synthesis of encapsulated copper nanoparticles using a hydroalcoholic extract of Moringa oleifera leaves and assessment of their antioxidant and antimicrobial activities. *Molecules*. 2020;25(3):555. doi:10.3390/molecules25030555
20. Clinical and Laboratory Standards Institute. *Reference Method for Broth Dilution Antifungal Susceptibility Testing of Yeasts (M27-A2)*. Malvern (PA): Clinical and Laboratory Standards Institute; 2002.
21. Zeebaree AYS, Zeebaree SYS, Rashid RF, et al. Sustainable engineering of plant-synthesized TiO2 nanocatalysts: diagnosis, properties and their photocatalytic performance in removing of methylene blue dye from effluent: a review. *Curr Res Green Sustain Chem*. 2022;5:100312. doi:10.1016/j.crgsc.2022.100312
22. Shiraz M, Imtiaz H, Azam A, Hayat S. Phytogenic nanoparticles: synthesis, characterization, and their roles in physiology and biochemistry of plants. *Biometals*. 2024;37(1):23–70. doi:10.1007/s10534-023-00542-5
23. Schlichter Kadosh Y, Goorevitch N, Teralı K, Gopas J, Kushmaro A. Nebivolol, an FDA-approved drug, has general antibacterial and antibiofilm effects and increases Pseudomonas aeruginosa tolerance to ciprofloxacin. *Pharmaceuticals*. 2024;17(11):1472. doi:10.3390/ph17111472
24. Mackenzie DWR. Serum tube identification of Candida albicans. *J Clin Pathol*. 1962;15:563–565. doi:10.1136/jcp.15.6.563
25. Gebarowska E, Lyczko J, Rdzanek M, et al. Evaluation of antimicrobial and chemopreventive properties and phytochemical analysis of Solanum nigrum L. aerial parts and root extracts. *Appl Sci*. 2022;12(14):6845. doi:10.3390/app12146845
26. International Organization for Standardization. *ISO 10993-4:2017. Biological Evaluation of Medical devices—Part 4: Selection of Tests for Interactions with Blood*. Geneva: ISO; 2017.
27. Bai B, Saranya S, Dheepaasri V, et al. Biosynthesized copper oxide nanoparticles (CuO NPs) enhances the anti-biofilm efficacy against K. pneumoniae and S. aureus. *J King Saud Univ Sci*. 2022;34(6):102120. doi:10.1016/j.jksus.2022.102120
28. Padmavathi AR, SM P, Das A, et al. Impediment to growth and yeast-to-hyphae transition in Candida albicans by copper oxide nanoparticles. *Biofouling*. 2020;36(1):56–72. doi:10.1080/08927014.2020.1715371
29. Akinosoglou K, Livieratos A, Asimos K, Donders F, Donders GG. Fluconazole-resistant vulvovaginal candidosis: an update on current management. *Pharmaceutics*. 2024;16(12):1555. doi:10.3390/pharmaceutics16121555
30. Carmo PHFD, Garcia MT, Figueiredo-Godoi LMA, Lage ACP, Silva NSD, Junqueira JC. Metal nanoparticles to combat Candida albicans infections: an update. *Microorganisms*. 2023;11(1):138. doi:10.3390/microorganisms11010138
31. Fan F, Liu Y, Liu Y, et al. Candida albicans biofilms: antifungal resistance, immune evasion, and emerging therapeutic strategies. *Int J Antimicrob Agents*. 2022;60(5–6):106673. doi:10.1016/j.ijantimicag.2022.106673
32. Jalal M, Ansari MA, Alzohairy MA, et al. Anticandidal activity of biosynthesized silver nanoparticles: effect on growth, cell morphology, and key virulence attributes of Candida species. *Int J Nanomed*. 2019;Volume 14:4667–4679. doi:10.2147/IJN.S210449
33. Mudiar R, Kelkar-Mane V. Targeting fungal menace through copper nanoparticles and Tamrajal. *J Ayurveda Integr Med*. 2020;11(3):316–321. doi:10.1016/j.jaim.2018.02.134
34. Khalaf HY, Nasr FB, Noomi BS, Mnif S, Aifa S. Assessing the efficacy of chemical and green-synthesized CuO nanoparticles in combatting clinical Candida species: a comparative study. *Microbiology Res*. 2025;16(8):178. doi:10.3390/microbiolres16080178
35. Karimiyan A, Najafzadeh H, Ghorbanpour M, Hekmati-Moghaddam SH. Antifungal effect of magnesium oxide, zinc oxide, silicon oxide and copper oxide nanoparticles against Candida albicans. *Zahedan J Res Med Sci*. 2015;17(10). doi:10.17795/zjrms-2179
36. Monteiro DR, Gorup LF, Silva S, et al. Silver colloidal nanoparticles: antifungal effect against adhered cells and biofilms of Candida albicans and Candida glabrata. *Biofouling*. 2011;27(7):711–719. doi:10.1080/08927014.2011.599101
37. Aghaei M, Kianpour M, Mardanian F, Farahbod F, Fahami F, Ghahremantermeh M. Evaluation of the therapeutic effect of 15 ppm silver nanoparticle spray compared to clotrimazole 1% on candida vaginitis: a randomized controlled clinical trial. *J Family Reprod Health*. 2023;17(4):255. doi:10.18502/jfrh.v17i4.14598
38. Hosseini SS, Joshaghani H, Shokohi T, Ahmadi A, Mehrbakhsh Z. Antifungal activity of ZnO nanoparticles and nystatin and downregulation of SAP1-3 genes expression in fluconazole-resistant Candida albicans isolates from vulvovaginal candidiasis. *Infect Drug Resist*. 2020;Volume 13:385–394. doi:10.2147/IDR.S226154
39. El-Sherbiny GM, Shehata ME, Kalaba MH. Biogenic copper and copper oxide nanoparticles to combat multidrug-resistant Staphylococcus aureus: green synthesis, mechanisms, resistance, and future perspectives. *Biotechnol Rep*. 2025;46:e00896. doi:10.1016/j.btre.2025.e00896
40. Djearamane S, Xiu LJ, Wong LS, et al. Antifungal properties of zinc oxide nanoparticles on Candida albicans. *Coatings*. 2022;12(12):1864. doi:10.3390/coatings12121864
41. Devaraji M, Thanikachalam PV, Elumalai K. The potential of copper oxide nanoparticles in nanomedicine: a comprehensive review. *Biotechnol Notes*. 2024;5:80–99. doi:10.1016/j.biotno.2024.06.001